How to measure the ESR intensity of the Al centre in optically bleached coarse quartz grains for dating purpose?

Eslem Ben Arous, Mathieu Duttine, Mathieu Duval

How to measure the ESR intensity of the Al centre in optically bleached coarse quartz grains for dating purpose?

Eslem Ben Arous [a,b,c,*], Mathieu Duttine [d], Mathieu Duval [a,e,f]

[a] *Centro Nacional de Investigaci´on Sobre La Evoluci´on Humana (CENIEH), Burgos, Spain*
[b] *Max Planck Institute of Geoanthropology, Pan-African Evolution Research Group, Jena, Germany*
[c] *Museum National d'Histoire Naturelle, Histoire Naturelle de L'Homme Préhistorique, Paris, France*
[d] *Institut de Chimie de La Matière Condensée de Bordeaux (ICMCB), Univ. Bordeaux, CNRS, Bordeaux INP, Pessac, France*
[e] *Australian Research Centre for Human Evolution (ARCHE), Griffith University, Brisbane, Australia*
[f] *Palaeoscience Labs, Dept. Archaeology and History, La Trobe University, Melbourne Campus, Bundoora, Victoria, Australia*

A B S T R A C T

The ESR intensity of the Al signal has been traditionally extracted from the measurement of the amplitude be- tween the top of the first peak and the bottom of the last peak from g = 2.0185 to g = 1.9928. However, a recent study by Kabacin´ska and Timar-Gabor (2022) showed the limitations of this method. As a follow-up, we investigated and compared various Al signal intensity extraction methods to evaluate their impact on the De estimation of several coarse-grained quartz samples (100–200 μm) from Early Pleistocene to modern-age deposits.

In particular, we tested the potential of using the area of the Al signal near g = 2.0603, as it is theoretically free of any major interfering signals. However, our results show that the extraction methods related to this area do not offer any substantial advantages over the traditional method in the case of coarse-grained samples. Instead, measurement of the ESR intensity is more time consuming, and resulting dose response curves are more scattered. Actually, most Al intensity extraction methods tested in this study return equivalent dose (De) estimates (as well as bleaching coefficient values) within error, suggesting that the interfering signals do not seem to strongly bias the ESR dose evaluation in those coarse-grained quartz samples. This outcome provides additional support in favor of the use of the traditional method. However, the significant inter-sample variability observed in our study nevertheless shows the necessity to extend this investigation to a larger number of samples of various grain sizes, origins and chronologies in order to identify more meaningful patterns on a larger scale.

1. Introduction

Electron Spin Resonance (ESR) belongs to the trapped-charge dating methods and has been extensively used over the last 40 years on optically-bleached quartz grains to chronologically constrain Pleistocene archaeo-palaeontological sites and fluvial terrace deposits (Bartz et al., 2018; Duval et al., 2020; Falguères, 2020; Ingicco et al., 2018; Parés et al., 2021; Voinchet et al., 2020). Since the pioneering study by Yokoyama et al. (1985), ESR dating of quartz has been mostly based on the measurement of the radiation-induced signal coming from the aluminium (Al) hole centre $[AlO_4]^0$, while the use of the various titanium (Ti) centres ($[TiO_4/M^+]^0$, with M = Li, H or Na) has only become increasingly popular about a couple of decades later through the Multiple Centre (MC) approach (Toyoda et al., 2000). Although these Ti centres show full signal reset and much faster bleaching kinetics compared to the Al centre (e.g., Duval et al., 2017; Tissoux et al., 2007; Toyoda et al., 2000), the latter is usually easier to measure. Associated with the most abundant trace element in α-quartz (Preusser et al., 2009), the Al signal typically shows a much stronger ESR intensity and requires much shorter measurement time to obtain a spectrum with acceptable signal-to-noise ratio (Duval, 2012; Duval and Guilarte, 2015; Tissoux et al., 2015; Voinchet et al., 2010).

Traditionally, the ESR intensity of the Al signal has been extracted from a peak-to-peak amplitude measurement following Yokoyama et al. (1985). However, the possibility of other alternative measurement procedures has been very little investigated so far, until the recent paper

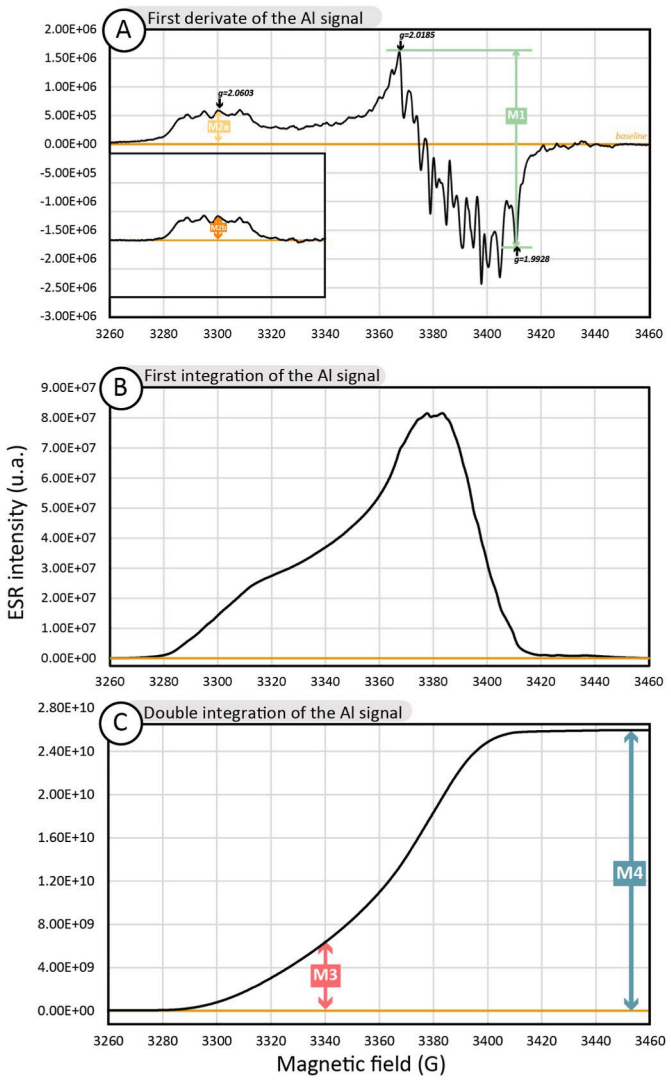

Fig. 1. The four methods used in this study to extract the Al intensities. A: First derivate the Al signal with Method 1, Method 2a and Method 2b; B: first integration of the Al signal; C: Double integration of the Al signal illustrating Method 3 and 4. Key: M1: peak-to-peak amplitude (Yokoyama et al., 1985); M2a: peak-to-baseline amplitude (Kabacińska and Timar-Gabor, 2022); M2b: peak-to-baseline amplitude (this study); M3: double integration of the signal from the area used for M2a-b (this study); M4: double integration of the whole Al signal (this study).

by Kabacińska and Timar-Gabor (2022), which strongly questioned the validity of the traditional approach. As a follow-up on this earlier work, we conducted the first comparative study based on a range of coarse quartz grain samples (120–200 μm) from Early Pleistocene to modern-age sediment to determine and discuss the most appropriate way to measure the ESR intensity of the Al signal. Several measurement procedures were tested, and implications regarding bleaching rates and equivalent dose determination are discussed.

2. Background

According to the basics of quantitative ESR studies, the number of unpaired spins increases during the irradiation and is proportional to the area under the absorption curve (e.g., Burns and Flockhart, 1990; Eaton et al., 2010). Therefore, since the ESR spectra are being recorded in their first-derivative form, the ESR intensity should, in theory, be extracted from the double integration of the signal. However, in the case of ESR dose reconstruction studies, the intensity can also be measured from the peak-to-peak amplitude of the signal, since signals of similar shape are being compared (Burns and Flockhart, 1990).

In ESR dating of quartz grains, the pioneering work by Yokoyama et al. (1985) and the subsequent studies by Toyoda and Falguères (2003) and Lin et al. (2006) evaluated various peak-to-peak amplitude procedures for the measurement of the Al signal intensity and reached similar conclusions: they all recommended the use of the peak-to-peak amplitude between the top of the first peak and the bottom of the last peak from g = 2.0185 to g = 1.9928 (so-called Method 1 in the present study, Fig. 1). According to these works, the interfering signals present in that area, and which are positioned right in the middle of the Al signal, do not impact the resulting dose estimates. These so-called interfering signals can usually be identified at room temperature (~295 K), when Al centre signal is not detectable. One of the most commonly described in the literature is the OHC (oxygen hole centre) but the identification of the corresponding signals and g factors is difficult. According to Ikeya (1993), the signal of the peroxy centre NBOHC (corresponding to the "wet" OHC) is characterized by 3 g-factors (g_1 = 2.0010, g_2 = 2.0095, g_3 = 2.0078; Ikeya, 1993). Regarding the "dry" OHC (Stapelbroek et al., 1979; Toyoda, 2015) among the 3 g-factors described by Ikeya (1993) (g = 2.0014, g = 2.0074, g = 2.067), only g = 2.0074 is visible in natural quartz (Ikeya, 1993; Toyoda, 2015). Two others paramagnetic centres are typically reported in quartz and can only be measured at room temperature: Germanium (Ge) and E'_1. They both show a limited potential for dating purpose. The first one is radiation-sensitive, but can hardly be observed in natural samples because of its low thermal stability (Ikeya, 1993; McMorris, 1971). The second one is an oxygen vacancy centre (g_1 = 2.00179, g_2 = 2.00053, g_3 = 2.00030; Ikeya, 1993) and shows a non-monotonic dependence to temperature and sunlight exposure (Toyoda, 2005; Weeks and Nelson, 1960; Wei et al., 2019).

A recent study by Kabacińska and Timar-Gabor (2022) based on a combination of experiment and simulated ESR spectra from three loess samples suggested that these interfering signals could actually induce an overestimation of the Al signal intensity measured through the traditional approach. While the authors also acknowledged that such bias

Table 1
List of samples analyzed in this study with their corresponding context and estimated chronology. The modern-age sample #1 was given a pre-dose of 300 Gy, before applying the multiple aliquot additive dose method (unpublished data).

ID	Sample	Locality or area, Country	Context	Chronology	Reference
#1	OUC1102-300	Oued Charef, Morocco	Fluvial (open air)	Modern (pre-dose = 300 Gy)	Sala-Ramos et al. (2022)
#2	KT04/2/2	Southern Cape, South Africa	Aeolian dune	~50 ka	Ben Arous et al. (2022)
#3	SF05-2-4	Southern Cape, South Africa	Aeolian dune	Modern	Ben Arous et al. (2022)
#4	CAC1203	Base Menacho, Spain	Fluvial (open air)	~20 ka	García-Vadillo et al. (2021)
#5	CUB1004	Cuesta de la Bajada, Spain	Fluvial (open air)	~300 ka	Duval et al. (2017)
#6	ALC1201	Alcanadre river terrace, Spain	Fluvial (open air)	~1.2 Ma	Duval et al. (2015)
#7	GD1405	Atapuerca Gran Dolina TD1, Spain	Fluvial (karst)	~1.2 Ma	Duval et al. (2020)
#8	LC09/1/02	Southern Cape, South Africa	Aeolian dune	>149 ka	Ben Arous et al. (2022)
#9	MOR1101	Morée-Villeprovert, France	Fluvial (open air)	Middle Pleistocene	Duval et al. (2017)
#10	FN10001	Fuente Nueva 3, Spain	Fluvio-lacustrine (open air)	Early Pleistocene	Duval et al. (2017)

Table 2
Comparison of the D_e values obtained with the four intensity measurement methods. ESR fitting results using a DSE function through the experimental data points. The ESR intensity of the residual, unbleachable component was not subtracted. Initial fitting carried out for samples #5 and #7 returned results with unusually large errors and was most likely biased by the presence of one outlier in the DRC. Consequently, additional fitting was carried out without this experimental point, returning more reliable fitting results (in italics).

ID	Sample	Fitting function	M1	adj-r^2	M2a	adj-r^2	M2b	adj-r^2	M3	adj-r^2	M4	adj-r^2
1	OUC1102-300	DSE(W-1/I^2)	313 ± 58	0.985	465 ± 84	0.995	505 ± 91	0.994	575 ± 90	0.994	498 ± 65	0.997
2	KT04-4	DSE(W-1/I^2)	40 ± 5	0.996	39 ± 5	0.996	69 ± 11	0.991	31 ± 5	0.993	32 ± 2	0.994
3	SF05-2-4	DSE(W-1/I^2)	211 ± 53	0.992	161 ± 70	0.982	186 ± 38	0.993	188 ± 59	0.987	176 ± 43	0.992
4	CAC1203	DSE(W-1/I^2)	255 ± 27	0.997	228 ± 24	0.997	242 ± 45	0.992	254 ± 37	0.995	253 ± 25	0.997
5	CU1004[a]	DSE(W-1/I^2)	723 ± 306	0.997	400 ± 180	0.998	423 ± 677	0.994	785 ± 342	0.997	482 ± 193	0.997
			799 ± 229	*0.999*	*553 ± 95*	*0.999*	*797 ± 319*	*0.998*	*825 ± 225*	*0.998*	*603 ± 120*	*0.999*
6	ALC1201	DSE(W-1/I^2)	780 ± 208	0.998	1293 ± 221	0.998	1756 ± 317	0.998	1658 ± 357	0.997	1053 ± 204	0.998
7	GD1405[b]	DSE(W-1/I^2)	4170 ± 1238	0.992	3175 ± 887	0.988	3779 ± 1515	0.984	5845 ± 2359	0.979	2601 ± 853	0.985
			4032 ± 638	*0.997*	*3741 ± 606*	*0.994*	*3840 ± 2036*	*0.987*	*3285 ± 2125*	*0.981*	*3356 ± 651*	*0.991*
8	LC09	DSE(W-1/I^2)	394 ± 128	0.992	735 ± 151	0.992	735 ± 151	0.992	449 ± 125	0.992	652 ± 147	0.992

[a] For sample #5, data in italics were calculated without the irradiated point at 1000 Gy.
[b] For sample #7, data in italics were calculated without the irradiated point at 8000 Gy.

could be sample dependent, this overestimation seems to be overall higher on fine grains (4–11 μm) than on coarse grains (>120 μm). For this reason, they recommended using instead the peak-to-baseline amplitude measurement of the absorption lines around g = 2.0603 (Method 2, Fig. 1) after a baseline correction of the whole Al signal. While these authors also suggested that using a double integration of the first derivative Al signal would be a more appropriate way to extract the Al intensities, in agreement with Eaton et al. (2010), they did not test it. Moreover, as an additional issue against the use of the peak-to-peak amplitude measurements, previous studies have highlighted the variability of the Al signal among samples of different origins in terms of the number of peaks (e.g., Lin et al., 2006 and references therein), which might potentially impact resulting dose estimates. Theoretically, the area around g = 2.0603 should be free of interfering signals, and using the double integration of the first-derivative signal of this specific area may be of greater potential for dose evaluation, as suggested earlier by Duttine (2005).

3. Material and method

3.1. Samples

Ten coarse-grained quartz samples (named #1 to #10) were selected from previous dating application studies (Arnold et al., 2016; Bateman et al., 2011; Ben Arous et al., 2022; Demuro et al., 2020; Duval et al., 2015, 2017; García-Vadillo et al., 2021; Méndez-Quintas et al., 2018; Sala-Ramos et al., 2022). Samples #1 to # 8 are used for the comparison of the equivalent dose (D_e) values derived from each method (section 3). They cover a wide range of chronologies and origins (Table 1). The discussion around the implications for bleaching rates is based on the last two samples #9 and #10, for which we have bleaching curves with a high density of data points (Duval et al., 2017).

3.2. Measurement conditions

Al signals were measured at cryogenic temperatures (~90 K) with an EMXmicro 6/1Bruker X-band ESR spectrometer coupled to a standard rectangular ER 4102ST cavity (so-called setup #1 in Guilarte and Duval, 2021). The following acquisition parameters were employed: 1 scan, 10 mW microwave power, 1024 points resolution, 100 kHz modulation frequency, 0.1 mT modulation amplitude, 40 ms conversion time, 10 ms time constant, and 40 s sweep time. Each aliquot was measured after three rotations of ~120° in the cavity to consider the angular dependence of the signal due to sample heterogeneity. While all samples were repeatedly measured 2 or 3 times over successive days, we only processed the ESR data from the first measurement time for the present study. Further information about measurement conditions may be found in Table 1 and references therein.

Additionally, the natural aliquot of samples #1 to #8 was specifically re-measured at ambient (297 K) and cryogenic (90 K) temperatures in order to visualize and identify the interfering signals. The following acquisition parameters were employed: 1–20 scans, 10 mW microwave power, 2048 points resolution, 100 kHz modulation frequency, 0.1 mT modulation amplitude, 40 ms conversion time, 10 ms time constant.

3.3. Extraction of the Al ESR intensities

Four methods were employed (Fig. 1). Method 1 (M1) is the traditional peak-to-peak amplitude measurement between the top of the 1st peak and the bottom of the 16th peak from g = 2.0185 to g = 1.9928 initially proposed by Yokoyama et al. (1985). Method 2 (M2) is divided into two sub-methods 2a and 2b. Method 2a refers to the approach developed by Kabacińska and Timar-Gabor (2022), and the Al intensities are measured from the peak-to-baseline amplitude of the signal around g = 2.0603. When necessary, a previous baseline correction of the whole spectrum was applied. This approach is justified by the fact that this part of the Al signal is supposedly free of any interference from the peroxy signals. In Kabacińska and Timar-Gabor (2022), the intensity amplitude was systematically measured from a specific point located between two middle peaks in the area of g = 2.0603. However, this point is not always visible for all the samples, and especially for the bleached and natural aliquots. In our study, we used instead the second peak as the reference point (Fig. 1A). Method 2b uses the same area of the Al signal as M2a, with a local correction of the baseline using a cubic function applied to all spectra in the magnetic field intervals 3260–3275 and 3329–3350 G to ensure comparability. Method 3 (M3) follows the recommendation of Duttine (2005): rather than the peak-to-baseline amplitude measurement of the M2, we performed the double integration of the low-field component around g = 2.0603 from 3260 to 3340 G. Finally, Method 4 (M4) is based on the double integration of the whole Al signal (Fig. 1C).

3.4. Equivalent dose determination

All ESR intensities were corrected by their corresponding receiver gain value, temperature factor (Duval and Guilarte Moreno, 2012), number of scans and aliquot mass. In order to compare the dose response curves (DRC) derived from each method for one given sample, the Al intensities were systematically normalized by the intensity of the natural aliquot. DRC fitting was carried out with Origin Pro 8 (OriginLab Corporation, Northampton, USA) using a Levenberg Marquardt algorithm by chi-square minimization. The ESR intensity and associated experimental error obtained for each point correspond to the mean value and standard deviation derived from the three rotations of the tube performed for each aliquot measured. Dose response Curve (DRC) fitting was performed using a Double Saturating Exponential (DSE) function

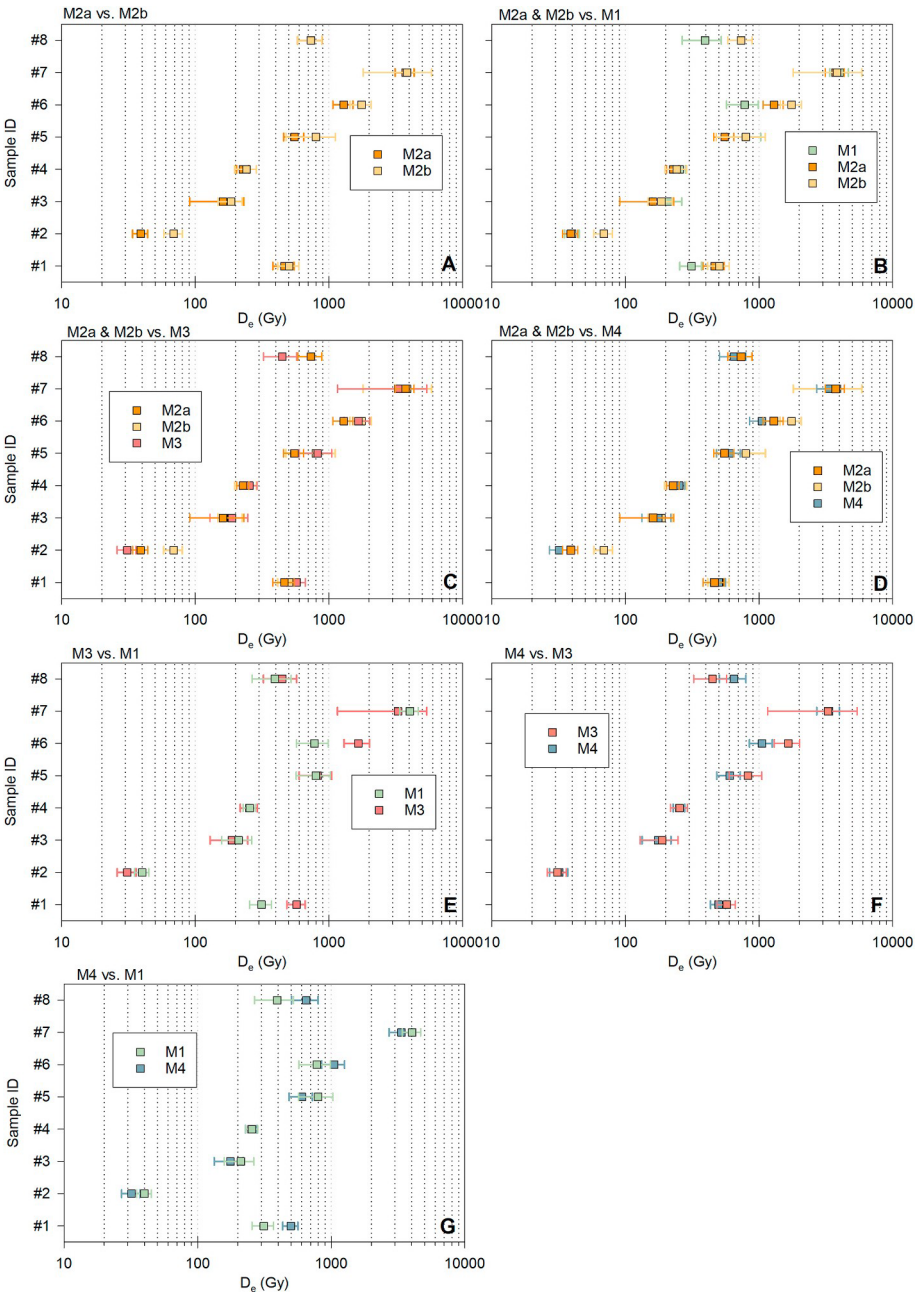

Fig. 2. Comparison of the D_e values obtained with the four methods. D_e are represented with 1 sigma error.

(Duval et al., 2009) with data weighted by $1/I^2$ (I = ESR intensities). All DRCs are provided in Supplementary Material (Fig. S1 to Fig. S8).

4. Results and discussion

4.1. ESR signals

Fig. S9, S10 and S11-A to S18-A show the existing variability of the ESR signal among samples, or even among aliquots of a given sample. For example, a limited, but non-negligible, shift of a few Gauss (G) in the position of the first (<3 G) and last (<5 G) peaks in the g = 2.02–1.99 area may be observed. The number of peaks composing the Al signal in that area is also quite variable: while previous works have been reporting some differences (e.g., 16 peaks identified by Yokoyama et al., 1985, 14 by Lin et al., 2006), we cannot exclude that part of this difference might result from distinct counting methods. Consequently, to avoid any methodological bias, we performed our own counting by considering each negative (bottom) or positive peak (top) of the first-derivative Al ESR signal of our samples (Supplementary Material, Fig. S10), and extended this comparison to other samples from previous works (Yokoyama et al., 1985; Lin et al., 2006; Kabacińska and Timar-Gabor, 2022). Overall, the total number of peaks ranges from 16 to 28, although the large majority of the samples (9/13) shows little variation between 24 and 28 peaks (Supplementary Material, Table S1). Interestingly, the three loess samples from Kabacińska and Timar-Gabor (2022) show the smaller number of peaks: 16 for 2 MV 80 (63–90 μm), and 20–22 for STY 1.10 and ROX 1.14. In comparison, the other two samples with a grain size partly or totally <100 μm show 24 peaks, suggesting that the lower number of peaks is not resulting from a smaller grain size. While we cannot exclude that our peak counting might be partly biased by the low resolution of the published natural aliquot spectra displayed in Kabacińska and Timar-Gabor (2022), the difference

Table 3
Comparison of bleaching coefficient values calculated from the different methods for each sample. The bleaching coefficient (Bl. coeff.) corresponds to the relative difference between the ESR intensity of the natural and bleached aliquots. AVG ± SD: average value and associated one standard deviation for a given sample or method.

ID	Sample	M1	M2a	M2b	M3	M4	AVG ± SD
1	OUC1102-300	51.3%	52.1%	49.0%	49.1%	53.4%	51.0 ± 1.9%
2	KT04-4	31.8%	32.8%	38.9%	34.8%	28.6%	33.4 ± 3.8%
3	SF05-2-4	22.4%	29.5%	29.1%	27.9%	34.5%	28.7 ± 4.3%
4	CAC1203	42.3%	40.4%	42.6%	47.1%	38.8%	42.2 ± 3.1%
5	CU1004	55.7%	57.4%	57.4%	56.9%	58.2%	57.1 ± 0.9%
6	ALC1201	60.2%	62.1%	63.1%	61.9%	60.0%	61.5 ± 1.3%
7	GD1405	53.3%	56.7%	55.1%	52.6%	54.9%	54.5 ± 1.6%
8	LC09	41.9%	42.7%	43.4%	46.5%	46.6%	44.2 ± 2.2%
	AVG ± SD	44.9 ± 12.9%	46.7 ± 12.1%	47.3 ± 11.0%	47.1 ± 11.1%	46.9 ± 11.7%	

is unlikely to originate from the experimental conditions, which are very similar (e.g., measurement temperature of 90 K, modulation amplitude of 1G, modulation frequency of 100 kHz and microwave power of 2 mW). (Supplementary Material, Fig. S11-B to S18-B). The only noticeable effect is the noisier spectrum obtained at 2 mW. Consequently, the most plausible explanation is that the variability observed in the number of peaks of the Al signal between the three loess samples analyzed by Kabacińska and Timar-Gabor (2022) and the other samples is most likely related to the magnitude and nature of the interfering signals. Actually, Timar-Gabor (2018) observed an inverse correlation between the ESR intensity and the grain size, the intensity of E'_1 and peroxy signals being stronger in finer grains.

The natural spectrum (Figs. S11–S18) of the 8 samples shows that interfering signals are visible at room temperature (297 K), and a relatively weak intensity compared to the Al signal at cryogenic temperature. However, since the intensity of peroxy signal is also temperature dependent, the intensity of the signals observed at room temperature is not directly comparable to that obtained at 90 K. For most samples, these interfering signals (Figs. S11–S18) are mainly due to the NBOHC peroxy (corresponding to the "wet" OHC; $g_1 = 2.049$; $g_2 = 2.0079$; $g_3 = 2.0032$) and E'_1 (only two g-values are clearly visible: $g_1 = 2.0018$; $g_2 = 2.0007$, the latest may correspond to two components with very similar g-values) centres, while other centres may sometimes be also observed, e.g.: Ge/Li ($g_1 = 1.999$; $g_2 = 1.9973$; $g_3 = 1.9962$), OHC ($g = 2.011$) and SO^- ($g = 2.0028$; $g// = 2.0032$). However, since these several signals may overlap, it is difficult to extract exact g-values, as they may slightly differ from those available in the literature (Ikeya, 1993; Toyoda et al., 2000; Duttine, 2005). Relatively speaking, we observe that the ESR intensity of the peroxy signals is slightly higher for the youngest samples (#1 to #4), i.e for which the Al signals are weaker (Supplementary Material, Figs. S11–S18). Additional acquisitions performed with a microwave power of 2 mW as in Kabacińska and Timar-Gabor (2022) show that the amplitude of the interfering signals in samples #2 to #4 is higher with 2 mW than with 10 mW (i.e, the microwave power used in the present study), suggesting some microwave saturation effects of these signals (Supplementary Material, Fig. S11-B to S18-B).

4.2. Comparison of the equivalent dose values

4.2.1. M2a vs M2b

M2b D_e estimates are systematically higher (24% on average) than M2a results (Table 2, Fig. 2-A), thus suggesting a non-negligible influence of the baseline correction on the resulting dose estimates. However, the significance of this systematic bias is somewhat weakened by the fact that D_e results agree within 1σ error for 7/8 samples, the exception being sample #2. Without the latter, the M2b D_e overestimation drops to 16%.

4.2.2. M2a and M2b vs M1

No systematic bias is observed between M2a and M1 D_e estimates: three and five samples yield higher M2a and M1 D_e estimates, respectively (Table 2, Fig. 2-B). D_e estimates are nevertheless 1σ consistent for 5/8 samples. In comparison, M2b returns D_e values that are within close range to M1 results for half of the samples. For the four samples showing significant differences, the M2b approach systematically yields higher dose estimates. The systematic deviation of M2a and M2b with respect to M1 D_e values range from -46% to +44%, and -12% to +125%, resulting in average differences of -3% and +40%, respectively. In other words, the wide range covered by the systematic deviations shows the significant existing inter-sample variability, although average values suggest that M2a and M1 methods overall return somewhat close results, unlike for M2b compared to M1.

To sum up, the M1 D_e estimates are never higher than those obtained from M2a and M2b, and the dose overestimation supposedly produced by the interfering signals impacting the ESR intensity extracted from M1 method is not observed in our present data set. A couple of factors may explain this in apparent contradiction with the previous observations from Kabacińska and Timar-Gabor (2022). First, Kabacińska and Timar-Gabor (2022) investigated three grain size fractions (4–11, 63–90 and 125–180 μm), and most of the samples in their study belong to a finer fraction than in the present work (125–180 μm). They are therefore more likely to show a greater influence of the peroxy and E'_1 signals (see Timar-Gabor, 2018) than our samples. Second, the differences in the experimental conditions should probably also be considered. In particular, the E'_1 centre is known to saturate at relatively low microwave power (Timar-Gabor, 2018; Toyoda and Schwarcz, 1997): its intensity may significantly decrease above 0.5 mW, and the remaining signal above 10 mW is part of NBOHC (Ikeya, 1993). This may explain why the Al signal at 2 mW shows a greater influence of the interfering signals than at 10 mW for the samples showing the weakest Al signals (Supplementary Material, Fig. S11-B to S18-B).

4.2.3. M2a and M2b vs M3

No systematic bias is observed between M2a or M2b and M3 results: the latter returns either higher or lower values, depending on the sample considered. These differences range from -39% to +49% for M2a compared to M3 (+7% on average), and from -55 to +14% (-11% on average) for M2b with respect to M3 (Table 2, Fig. 2-C). Despite this apparent scatter, all but one D_e results are actually 1σ-consistent for a given sample. The exception is the M2b D_e results of 69 ± 11 Gy for sample #2, which should be regarded as an outlier: the D_e value is significantly higher than any other D_e results, which range between 30 and 40 Gy, regardless of the method considered (Table 2). Additionally, the spectra are noisy, as shown with the natural spectrum of sample #2 (Figs. S12–A), making it difficult to extract intensities without high variability, as can be shown with the associated low adjusted r^2 value of 0.991. Consequently, the three methods M2a, M2b and M3 return somewhat close dose results on average. As far as goodness-of-fit, M2a returns on average slightly higher adjusted r^2 values than M2b and M3 ($0.994 > 0.993 > 0.992$).

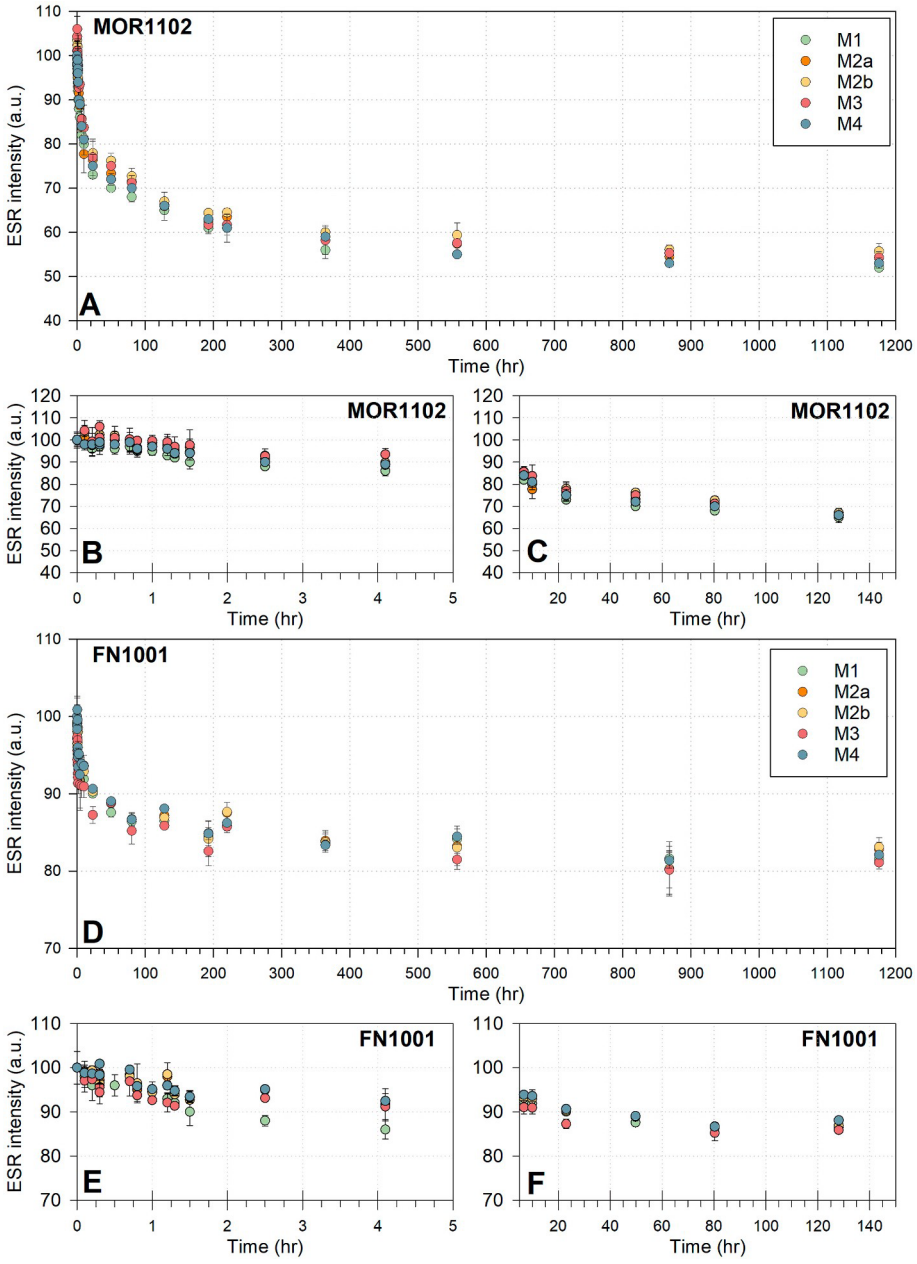

Fig. 3. Evolution of the Al signal intensity along with UV exposure. ESR intensities were evaluated through Methods 1, 2a, 2b, 3 and 4. Original ESR data set (M1) from Duval et al. (2017). Al signal bleaching kinetics of the sample #9 (MOR1102) and sample #10 (FN10001) is displayed between 0 and 1200 h (A and D), 0 and 5 h (B and E), and between 5 and 150 h (C and F).

4.2.4. M2a and M2b vs M4

M2a and M4 return close dose estimates (Table 2, Fig. 2-D). The difference is of only 4% on average, and all samples provide D_e values within 1σ error. In comparison, M2b and M4 show larger differences, with M2b yielding D_e values higher by +18% on average (without considering sample #2), and 7/8 samples providing consistent D_e results. Interestingly, these results suggest that interfering signals do not significantly impact the dose estimates obtained from M4.

4.2.5. M3 vs M1

M1 and M3 D_e values are 1σ consistent for 6/8 samples, the exceptions being samples #1 and #6 (Table 2, Fig. 2-D). No apparent systematic deviation is observed between the methods. M1 also provides on average a higher goodness-of-fit than M3 (0.994 vs. 0.992).

4.2.6. M3 vs M4

M4 and M3 D_e values (Fig. 2-F) are 1σ consistent for 7/8 samples. No systematic deviation is observed between the two methods, which differ by only 4% on average. Goodness-of-fit achieved with M4 is on average higher than with M3 (0.995 vs. 0.992). This suggest that the interfering signals that might potentially affect the ESR intensity obtained from M4 do not have a significant impact on the resulting dose estimates.

4.2.7. M4 vs M1

No systematic deviation is observation between the two methods. M4 and M1 D_e values (Fig. 2-G) are 1σ consistent for 7/8 samples, and differ by 10% on average. This indicates that the traditional method (M1) and the double integration of the whole Al signal (M4) return very close results. Goodness-of-fit achieved by the two methods is similar on average (adjusted r^2 = 0.995).

4.3. Bleaching coefficient

The Al signal is characterized by a residual, unbleachable component, which is usually evaluated by exposing one aliquot to ultraviolet (UV) radiations in a solar simulator (Voinchet et al., 2003). The bleaching coefficient (expressed in %) corresponds to the relative difference between the ESR intensity of the bleached (I_b) and natural (I_n) aliquots, as follows: $(I_n - I_b)/I_n$.

The five methods yield close bleaching coefficient values: they vary by <5% for a given sample (Table 3), suggesting that the choice of the ESR intensity extraction method has very little impact on the calculated bleaching coefficient. However, one may notice a slight but systematic difference: while M2a, M2b, M3 and M4 return very close values on average (~47%), M1 yields smaller values by about 2% (~45%). This difference, however, might not be significant, as it falls within the standard experimental uncertainty on the ESR intensity (typically 1–2%; Duval et al., 2023).

4.4. Impact on bleaching rates

In order to evaluate the impact of the intensity measurement procedures on the bleaching rates of the Al signal, we re-analyzed the ESR spectra obtained from the bleaching experiment initially carried out by Duval et al. (2017). In that study, two quartz samples (MOR 1102 = sample #9; FN1001 = sample #10) were divided into multiple aliquots, which were bleached at increasing duration up to ~1200 h. New ESR intensities of the Al signal were extracted following the Methods 2a, 2b, 3, 4 and compared with the original data set (obtained from Method 1). Results are graphically displayed in Fig. 3.

For sample #9 (Fig. 3-A-B-C), the ESR intensities extracted from M2a, M2b, M3 and M4 differ on average by +2.7%, +4.6%, +4.8% and +2.1%, respectively, compared to the ESR intensities from M1. In contrast, sample #10 shows a distinct pattern (Fig. 3-D-E-F): on average, the M2a, M2b, M3 and M4 ESR intensities differ from M1 by +0.5%, +0.3%, +1.6% and +0.7%, respectively. In any case, the bleaching kinetics remain overall the same, regardless the measurement procedure. As of sample #9, all methods show a 19–29% decrease of the ESR intensity after 10 h, which reaches an apparent plateau around 360 h. Comparatively, sample #10 shows a somewhat different bleaching kinetics, although consistent for all methods, with a 7–10% decrease observed after 10 h, and minimum ESR intensities reached after ~190 h. These data illustrate the variability in the bleaching kinetics that may be observed among samples. In summary, the ESR intensity extraction method does not induce any major change in our knowledge of the Al signal bleaching kinetics, which is consistent with our previous observations on the bleaching coefficient values (section 3.3.).

5. Conclusions

As a follow-up on a previous work by Kabacińska and Timar-Gabor (2022) showing some limitations of the method traditionally employed (Toyoda and Falguères, 2003) to measure the ESR intensity of the Al signal (Method 1), we carried out a comparative study on several coarse-grained quartz samples. Various methods were tested, and perhaps the most striking observation is that the existing variability among samples is significant. This complicates the identification of clear patterns or of systematic deviations between methods. Following the recommendations by Kabacińska and Timar-Gabor (2022), we investigated the Al signal in the g = 2.0603 area and proposed two alternative options (M2b and M3) in addition to their intensity extraction method (M2a). However, they return D_e estimates that are within 1σ error with M2a for ~90% of the samples, suggesting that all methods return somewhat close results on average. Moreover, it is worth mentioning that M2a not only comparatively returns an overall slightly higher goodness-of-fit, but is also less time-consuming as far as data processing, as it does not require any baseline correction. To sum up, M2b and M3 do not offer any visible advantage over M2a for dose evaluation.

Our first results do not seem to confirm the initial observations by Kabacińska and Timar-Gabor (2022) about the interfering signals that may bias the ESR dose evaluation, leading to a dose overestimation. Actually, while M1 D_e estimates are within 1σ error with M2a, M2b and M3 dose values for the majority of the samples (>50%), they are unexpectedly lower when the difference becomes significant. This contradicts in first instance the previous observations by Kabacińska and Timar-Gabor (2022), although the authors also emphasized the significant variability of behaviors among samples. While we do not have a clear explanation for this pattern, we do nevertheless acknowledge that this apparent contraction may be related, at least partly, to the grain size of the samples being analyzed, inducing a more or less pronounced interference on the Al signal. As of now, our results do not unequivocally demonstrate the interest of preferring M2a, M2b or M3 over the traditional method for dose evaluation. However, the significant inter-sample variability observed in our study nevertheless shows the necessity to extend this investigation to a larger number of samples of various grain sizes, origins and chronologies in order to identify more meaningful patterns on a larger scale.

Declaration of competing interest

The authors declare that they have no known competing financial interests or personal relationships that could have appeared to influence the work reported in this paper.

Data availability

Data will be made available on request.

Acknowledgements

Spanish Ramón y Cajal Fellowship RYC2018-025221-I granted to MD is funded by MCIN/AEI/10.13039/501100011033 and by 'ESF Investing in your future. Aspects of this work is part of Grant PID2021-123092NB-C22 funded by MCIN/AEI/ 10.13039/501100011033/ 'ERDF A way of making Europe'. This study was part of the EBA's postdoctoral research, entirely funded by the Fyssen Foundation, to which she expresses her deepest thanks for its financial support. These results are part of a EBA's project that has received funding from the European Union's Horizon 2020 research and innovation programme under the Marie Skłodowska-Curie grant agreement No 101107408. We also warmly thank Maria Jesús Alonso Escarza for her huge support during the ESR data acquisition phase. Finally, we would like to thank two anonymous referees for their extensive and constructive comments that helped us to improve the later version of the manuscript.

References

Arnold, L.J., Duval, M., Demuro, M., Spooner, N.A., Santonja, M., Pérez-Gonzá lez, A., 2016. OSL dating of individual quartz 'supergrains' from the Ancient Middle Palaeolithic site of Cuesta de la Bajada, Spain. Quat. Geochronol. 36, 78–101. https://doi.org/10.1016/J.QUAGEO.2016.07.003.

Bartz, M., Rixhon, G., Duval, M., King, G.E., Álvarez Posada, C., Parés, J.M., Brückner, H., 2018. Successful combination of electron spin resonance, luminescence and palaeomagnetic dating methods allows reconstruction of the Pleistocene evolution of the lower Moulouya river (NE Morocco). Quat. Sci. Rev. 185, 153–171. https://doi.org/10.1016/J.QUASCIREV.2017.11.008.

Bateman, M.D., Carr, A.S., Dunajko, A.C., Holmes, P.J., Roberts, D.L., McLaren, S.J., Bryant, R.G., Marker, M.E., Murray-Wallace, C.V., 2011. The evolution of coastal barrier systems: a case study of the Middle-Late Pleistocene Wilderness barriers, South Africa. Quat. Sci. Rev. 30, 63–81. https://doi.org/10.1016/j. quascirev.2010.10.003.

Ben Arous, E., Duval, M., Bateman, M.D., 2022. ESR dating of optically bleached quartz grains from Plio-Pleistocene to Holocene coastal dune deposits (Wilderness-Knysna area, South Africa): a comparison with luminescence. Quat. Geochronol., 101293 https://doi.org/10.1016/j.quageo.2022.101293.

Burns, D.T., Flockhart, B.D., 1990. Application of quantitative EPR [and discussion]. Phil. Trans. Phys. Sci. Eng. 333 (1628), 37–48.

Demuro, M., Arnold, L.J., Duval, M., Méndez-Quintas, E., Santonja, M., Pérez-González, A., 2020. Refining the chronology of Acheulean deposits at Porto Maior in the River Miño basin (Galicia, Spain) using a comparative luminescence and ESR dating approach. Quat. Int. 556, 96–112.
https://doi.org/10.1016/j. quaint.2020.01.005.

Duttine, M., 2005. Recherche de provenance de quartz et d'obsidiennes préhistoriques en Europe occidentale: apports de la résonance paramagnétique électronique (RPE). In: Thése de doctorat, vol. 3. Universite de Bordeaux, Bordeaux.

Duval, M., 2012. Dose response curve of the ESR signal of Aluminum center in quartz grains extracted from sediment Dose response curve of the ESR signal of the Aluminum center in quartz grains extracted from sediment. Anc. TL 2, 1–10.

Duval, M., Arnold, L.J., Guilarte, V., Demuro, M., Santonja, M., Pérez-González, A., 2017. Electron spin resonance dating of optically bleached quartz grains from the Middle Palaeolithic site of Cuesta de la Bajada (Spain) using the multiple centres approach. Quat. Geochronol. 37, 82–96.
https://doi.org/10.1016/j.quageo.2016.09.006.

Duval, M., Arnold, L.J., Rixhon, G., 2020. Electron spin resonance (ESR) dating in Quaternary studies: evolution, recent advances and applications. Quat. Int. 556, 1–10.
https://doi.org/10.1016/j.quaint.2020.07.044.

Duval, M., Grün, R., Falguères, C., Bahain, J.J., Dolo, J.M., 2009. ESR dating of Lower Pleistocene fossil teeth: limits of the single saturating exponential (SSE) function for the equivalent dose determination. Radiat. Meas. 44, 477–482.
https://doi.org/10.1016/J.RADMEAS.2009.03.017.

Duval, M., Guilarte, V., Bartz, M., Alonso Escarza, M.J., Ben Arous, E., del Val, M., García Rodríguez, C., 2023. ESR dating of quartz grains: evaluating measurement repeatability and reproducibility. Radiat. Phys. Chem.
https://doi.org/10.1016/j. radphyschem.2023.111313.

Duval, M., Guilarte Moreno, V., 2012. Assessing the influence of the cavity temperature on the ESR signal of the Aluminum center in quartz grains extracted from sediment. Anc. TL 30, 11–16.

Duval, M., Guilarte, V., 2015. ESR dosimetry of optically bleached quartz grains extracted from Plio-Quaternary sediment: evaluating some key aspects of the ESR signals associated to the Ti-centers. Radiat. Meas. 78, 28–41.
https://doi.org/ 10.1016/j.radmeas.2014.10.002.

Duval, M., Sancho, C., Calle, M., Guilarte, V., Peña-Monné, J.L., 2015. On the interest of using the multiple center approach in ESR dating of optically bleached quartz grains: some examples from the Early Pleistocene terraces of the Alcanadre River (Ebro basin, Spain). Quat. Geochronol. 29, 58–69.
https://doi.org/10.1016/j. quageo.2015.06.006.

Eaton, G.R., Eaton, S.S., Barr, D.P., Weber, R.T., 2010. Quantitative EPR.

Falguères, C., 2020. A French story of the ESR dating method for Quaternary samples. Quat. Int. 556, 11–19.
https://doi.org/10.1016/j.quaint.2019.09.047.

García-Vadillo, F.-J., Duval, M., Canals-Salomó, A., Rodríguez-Álvarez, X.-P., Garcia- Garriga, J., Carbonell-Roura, E., 2021. Cuaternario y geomorfología. Cuaternario Geomorfol. 35, 147–174.

Guilarte, V., Duval, M., 2021. ESR dating of optically bleached quartz grains: intra- laboratory comparison of different experimental setups and their impact on dose evaluation. Geochronometria 48, 179–190.
https://doi.org/10.2478/geochr-2020-0005.

Ikeya, M., 1993. New Applications of Electron Spin Resonance: Dating, Dosimetry and Microscopy. World Scientific.

Ingicco, T., van den Bergh, G.D., Jago-on, C., Bahain, J.-J., Chacón, M.G., Amano, N., Forestier, H., King, C., Manalo, K., Nomade, S., Pereira, A., Reyes, M.C., Sémah, A.-M., Shao, Q., Voinchet, P., Falguères, C., Albers, P.C.H., Lising, M., Lyras, G., Yurnaldi, D., Rochette, P., Bautista, A., de Vos, J., 2018. Earliest known hominin activity in the Philippines by 709 thousand years ago. Nature 557, 233–237.
https:// doi.org/10.1038/s41586-018-0072-8.

Kabaciǹska, Z., Timar-Gabor, A., 2022, 2022. Dating Sediments by EPR Using Al-H Centre: A Comparison between the Properties of Fine (4-11 Microm) and Coarse (>63 Microm) Quartz Grains. Mol, vol. 27, p. 18. https://doi.org/10.3390/MOLECULES27092683. Page 2683 27.

Lin, M., Yin, G., Ding, Y., Cui, Y., Chen, K., Wu, C., Xu, L., 2006. Reliability study on ESR dating of the aluminum center in quartz. Radiat. Meas. 41, 1045–1049.
https://doi. org/10.1016/J.RADMEAS.2006.05.019.

McMorris, D., 1971. Impurity color centers in quartz and trapped electron dating: electron spin resonance, thermoluminescence studies. J. Geophys. Res. 76, 7875–7887.
https://doi.org/10.1029/JB076I032P07875.

Méndez-Quintas, E., Santonja, M., Pérez-González, A., Duval, M., Demuro, M., Arnold, L. J., 2018. First evidence of an extensive Acheulean large cutting tool accumulation in Europe from Porto Maior (Galicia, Spain). Sci. Rep. 8
https://doi.org/10.1038/ s41598-018-21320-1.

Parés, J.M., Duval, M., Soria-Jáuregui, A., González-Amuchástegui, M.J., 2021. First chronological constraints for the high terraces of the upper ebro catchment. Quaternary 4, 1–24.
https://doi.org/10.3390/QUAT4030025.

Preusser, F., Chithambo, M.L., Götte, T., Martini, M., Ramseyer, K., Sendezera, E.J., Susino, G.J., Wintle, A.G., 2009. Quartz as a natural luminescence dosimeter. Earth Sci. Rev. 97, 184–214.
https://doi.org/10.1016/J.EARSCIREV.2009.09.006.

Sala-Ramos, R., Chacón, M.G., Aouraghe, H., Haddoumi, H., Morales, J.-I., Rodríguez- Hidalgo, A., Tornero, C., Oujaa, A., Soto, M., Farkouch, M., Aissa, E.M., El Atmani, A., Duval, M., Arnold, L.J., Demuro, M., Blain, H.-A., Piñero, P., Rivals, F., Burjachs, F., Tarriño, A., Álvarez-Posada, C., Souhir, M., Saladié, P., Pla-Pueyo, S., Larrasoaña, J.C., Marín, J., Moreno, E., De Lombera-Hermida, A., Bartrolí, R., Lombao, D., García-Argudo, G., Ramírez, I., Díez-Canseco, C., Tomasso, S., Expósito, I., Allué, E., Noureddine, H., Mhamdi, H., Rhosne, H., Carrancho, A., Villalaín, J.J., Van der Made, J., Canals, A., Benito, A., Agustí, J., Parés, J.M., 2022. Evolución del asentamiento humano en la región de Aïn Beni Mathar – guefaït (Jerada, Marruecos Oriental). Investigaciones recientes en torno al poblamiento humano al norte del Sáhara. Takurunna 10–11, 179–203.

Stapelbroek, M., Griscom, D.L., Friebele, E.J., Sigel, G.H., 1979. Oxygen-associated trapped-hole centers in high-purity fused silicas. J. Non-Cryst. Solids 32, 313–326.
https://doi.org/10.1016/0022-3093(79)90079-6.

Timar-Gabor, A., 2018. Electron spin resonance characterisation of sedimentary quartz of different grain sizes. Radiat. Meas. 120, 59–65.
https://doi.org/10.1016/j. radmeas.2018.06.023.

Tissoux, H., Falguères, C., Voinchet, P., Toyoda, S., Bahain, J.J., Despriée, J., 2007. Potential use of Ti-center in ESR dating of fluvial sediment. Quat. Geochronol. 2, 367–372.
https://doi.org/10.1016/J.QUAGEO.2006.04.006.

Tissoux, H., Voinchet, P., Lacquement, F., Despriee, J., 2015. ESR as a method for the characterization of alluvial sediments. Radiat. Meas. 81, 2–8.
https://doi.org/ 10.1016/J.RADMEAS.2015.05.010.

Toyoda, S., 2015. Paramagnetic lattice defects in quartz for applications to ESR dating. Quat. Geochronol. 30, 498–505.
https://doi.org/10.1016/j.quageo.2015.05.010.

Toyoda, S., 2005. Formation and decay of the E1′ center and its precursor in natural quartz: basics and applications. Appl. Radiat. Isot. 62, 325–330.
https://doi.org/10.1016/J.APRADISO.2004.08.014.

Toyoda, S., Falguères, C., 2003. The method to represent the ESR signal intensity of the aluminium hole center in quartz for the purpose of dating. Adv. ESR Appl. 20, 7–10.

Toyoda, S., Schwarcz, H.P., 1997. Counterfeit E1′ signal in quartz. Radiat. Meas. 27, 59–66.
https://doi.org/10.1016/S1350-4487(96)00073-X.

Toyoda, S., Voinchet, P., Falgueres, C., Dolo, J.-M., Laurent, M., 2000. Bleaching of ESR signals by the sunlight : a laboratory experiment for establishing the ESR dating of sediments. Appl. Radiat. Isot. 52, 1357–1362.

Voinchet, P., Despriée, J., Tissoux, H., Falguères, C., Bahain, J.J., Gageonnet, R., Dépont, J., Dolo, J.M., 2010. ESR chronology of alluvial deposits and first human settlements of the Middle Loire Basin (Region Centre, France). Quat. Geochronol. 5, 381–384.
https://doi.org/10.1016/j.quageo.2009.03.005.

Voinchet, P., Falguères, C., Laurent, M., Toyoda, S., Bahain, J.J., Dolo, J.M., 2003. Artificial optical bleaching of the Aluminium center in quartz implications to ESR dating of sediments. Quat. Sci. Rev. 22, 1335–1338. https://doi.org/10.1016/ S0277-3791(03)00062-3.

Voinchet, P., Pereira, A., Nomade, S., Falguères, C., Biddittu, I., Piperno, M., Moncel, M. H., Bahain, J.J., 2020. ESR dating applied to optically bleached quartz - a comparison with 40Ar/39Ar chronologies on Italian Middle Pleistocene sequences. Quat. Int. 556, 113–123. https://doi.org/10.1016/j.quaint.2020.03.012.

Weeks, R.A., Nelson, C.M., 1960. Trapped electrons in irradiated quartz and silica: II, electron spin resonance. J. Am. Ceram. Soc. 43, 399–404. https://doi.org/10.1111/ J.1151-2916.1960.TB13682.X.

Wei, C.Y., Liu, C.R., Li, C.A., Yin, G.M., Zhang, Y.F., Li, W.P., Yu, L.P., 2019. Application of long time artificial optical bleaching of the E1' centre to sediment ESR dating. Geochronometria 46, 79–86. https://doi.org/10.1515/GEOCHR-2015-0106.

Yokoyama, Y., Falguères, C., Quaegebeur, J.P., 1985. ESR dating of quartz from Quaternary sediments : first attempts. Nucl. Tracks 10, 921–928.